Numerical investigation on the viewing angle of a lenticular three-dimensional display with a triplet lens array

Hwi Kim,[1,*] Joonku Hahn,[2] and Hee-Jin Choi[3]

[1]Department of Electronics and Information Engineering, College of Science and Technology, Korea University, Jochiwon-eup, Yeongi-gun, Chungnam 339-700, South Korea

[2]Department of Electrical and Computer Engineering, Duke University, Durham, North Carolina 27708, USA

[3]Department of Physics, Sejong University, Seoul 143-747, South Korea

*Corresponding author: hwikim@korea.ac.kr

Received 5 January 2011; revised 27 January 2011; accepted 28 January 2011; posted 31 January 2011 (Doc. ID 140385); published 1 April 2011

We investigate the viewing angle enhancement of a lenticular three-dimensional (3D) display with a triplet lens array. The theoretical limitations of the viewing angle and view number of the lenticular 3D display with the triplet lens array are analyzed numerically. For this, the genetic-algorithm-based design method of the triplet lens is developed. We show that a lenticular 3D display with viewing angle of 120° and 144 views without interview cross talk can be realized with the use of an optimally designed triplet lens array. © 2011 Optical Society of America

OCIS codes: 080.0080, 110.0110, 100.6890.

1. Introduction

Key requirements of a three-dimensional (3D) display for displaying natural 3D images are wide viewing angle and supermultiview angular resolution. A wide viewing angle 3D display is necessary for expressing the natural motion parallax of 3D images [1–6]. With respect to wide viewing angle 3D display technology, several 3D display architectures, such as the 360° light field volumetric display [1], wide viewing angle integral-imaging-based polyhedron display [2,6], wide viewing angle with curved devices [3,4], and a theoretical trial using a negative refractive lens [5], were reported. The human fatigue induced by the accommodation–vergence conflict under low angular resolution of a 3D display can be resolved by enhancing the angular resolution to the level of supermultiview resolution [7]. Projection-type 3D displays, such as the supermultiview projection 3D display [7] and the light field display known as HoloVizio [8], demonstrated high-quality 3D displays with highly enhanced angular resolution recently.

It can be said that the above-mentioned research has mainly focused on the aspects of system architecture. Among various 3D display architectures, the lenticular 3D display is the simplest structure that is composed of a periodic lens array and a 2D display panel [9–11]. In fact, without changing the display architecture any further, only the enhancement of the device performance of the lens array and the 2D display panel can greatly lead to high-performance lenticular 3D display. In general, novel functional devices for innovation of 3D displays must be developed.

In this paper, we investigate on the functional enhancement of the lens array, an elemental device of the lenticular 3D display, and its effect on display performance with numerical modeling and optimization techniques. The main point of our investigation is the use of the triplet lens array with reduced aberration for enhancing the viewing angle

0003-6935/11/111534-07$15.00/0

without interview cross talk by minimizing the lens aberration. The performance and its inherent limitations of the lenticular 3D display with the triplet lens array are discussed. In Section 2, the design procedure of the triplet lens based on the genetic algorithm for the 3D lenticular display is developed. In Section 3, the performance of the 3D unit pixel of the lenticular 3D display with designed triplet lens array is analyzed with numerical simulations. The concluding remarks are given in Section 4.

2. Aberration-Induced Interview Cross Talk in the Lenticular 3D Display

The basic structure of the lenticular 3D display is illustrated in Fig. 1(a). A periodic lens array is vertically aligned in front of a 2D display panel such as a liquid-crystal display (LCD). For this vertical lens scheme, the LCD with the mosaic pixel pattern is commonly used. The 3D unit pixel is referred to an effective pixel composed of a single lens and a finite number of pixels of the 2D LCD panel allocated to the single lens area. In Fig. 1(a), a 3D unit pixel is contrastively indicated by a shaded box where the single lens covers nine pixels horizontally. The pixel pitch, lens focal length, lens pitch, and optimal observation distance are denoted, respectively, by d, f, l, and h. The 3D unit pixel generates nine directional beams going to angularly separated spatial directions. An observer can identify angularly multiplexed pixel information through the 3D unit pixel by changing the observation angle θ_{ob}. As a result, nine separate images can be displayed directionally by this nine-view lenticular 3D display.

The maximum observation angle θ_{max} is defined by the angle between the normal vector and the observer position vector with the origin at the center of the lens when the view focus on the 2D display panel is put on the edge of the area of the 3D unit pixel. Thus the maximum observation angle θ_{max} is defined by $f_{eff} \sin\theta_{max} = Nd/2$ where N and d are the total number of views and the pixel pitch of the 2D LCD panel, respectively. The viewing angle $\theta_{v,max}$ is twice the number of the maximum observation angle θ_{max}. Thus the observer at the position of θ_{max} should see the magnified image of the local part of the first (leftmost) pixel of the 3D unit pixel under ideal conditions.

In the case of the lenticular 3D display, the viewing angle enhancement of the 3D displays is hindered by several factors from a technical viewpoint. Basically, the first factor is the limitation of the information capacity of 2D display panel. In principle, wide viewing angle 3D images can be displayed at the cost of resolution [2]. The second factor is the lens aberration, which produces viewing-angle-dependent cross talk. In general, in lens-based multiview autostereoscopic 3D displays as well as the lenticular 3D display, a high cross talk 3D unit pixel image is observed at a large viewing angle. The ray-tracing simulation results in Fig. 1(b) present the image cross talk induced by the lens aberration for the lenticular 3D display.

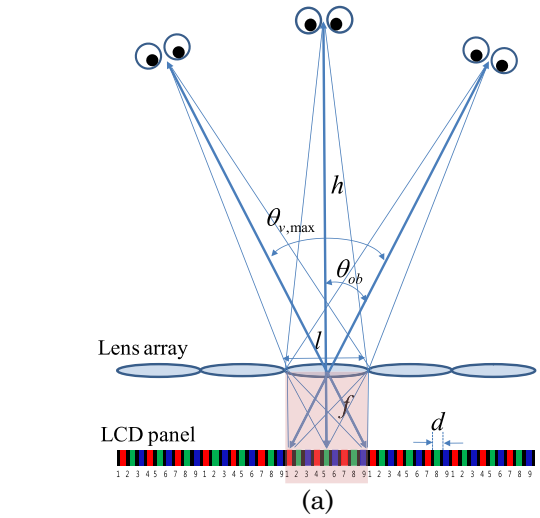

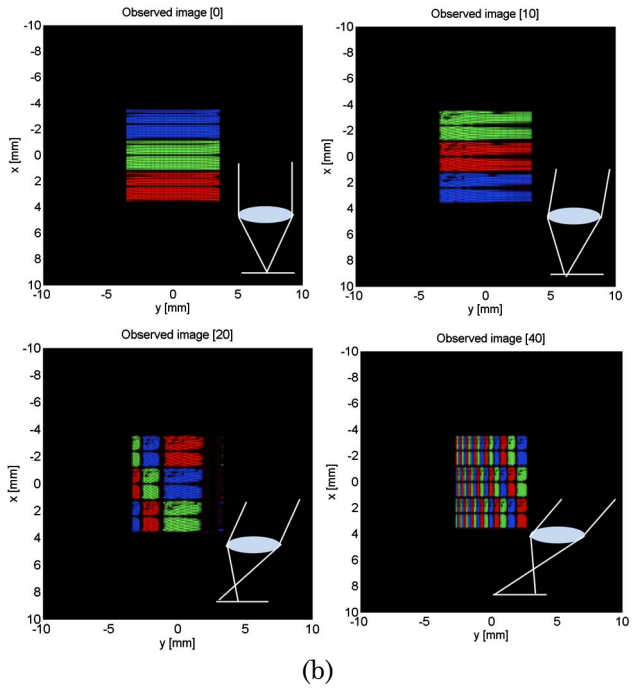

Fig. 1. (Color online) (a) Basic structure of the lenticular 3D display and (b) simulation images of the single 3D unit pixel observed at different observation viewing angles of 0°, 10°, 20°, and 40° obtained by a self-developed ray-tracing simulator.

The observer watching the 3D unit pixel along the normal direction to the lens aperture sees a magnified image of the pixel of the 2D panel behind the lens array as presented in the upper-left image in Fig. 1(b). As the viewing angle of the observer increases, more than one 2D pixels begin to be seen simultaneously to the observer. As manifested in the lower-right image in Fig. 1(b), at the observation angle of (b) 40°, the observed image of the 3D unit pixel is badly contaminated with interview cross talk. The lens aberration gives a serious limitation in 3D image quality and the viewing angle of the lenticular 3D display.

Considering a human eye with pupil diameter of 5 mm and interpupilary distance of 65 mm at an observation distance of 50 cm in front of a lenticular 3D display, we can evaluate the maximum acceptance angle of a human eye for supermultiview perception of about 0.5°, the convergence angle of 7.5°. Within this scheme, the 3D display modes of the lenticular 3D displays can be classified into the supermultiview mode with monocular parallax, binocular parallax mode, and multiview mode with no 3D effect. Figure 6 categorizes the exemplary 36 display schemes into these three display modes with respect to the viewing angle and the number of views of the lenticular 3D display. In this paper, the use of a triplet lens array is proposed as an innovation at the device level for a high-performance 3D lenticular display with a wide viewing angle and low cross talk. The 36 triplet lenses for the 36 cases in Fig. 6 are designed, and their display performances are investigated with numerical simulations in the following sections.

3. Design of the Triplet Lens Using the Genetic Algorithm

In this section, the optimal design method of a triplet lens is devised. The triplet lens is composed of six spherical optical surfaces, and its structure is specified by a total of 18 unknown structural variables as surface radii of optical layers r_i, refractive indices of optical layers n_i, and thickness of optical slayers d_i, as indicated in Fig. 2(a). Let us consider the point x_{inc} at the entrance pupil. The rays with the incidence angle of θ passing x_{inc} propagate through the lens system and strike a point at the focal plane, $x_o(x_{\text{inc}})$ that is a function of x_{inc}. An ideal triplet lens with an effective focal length f_{eff} would make a complete focus to a specific position of $x_o = f_{\text{eff}} \sin\theta$ for $-R \le \forall x_{\text{inc}} \le R$ where R is the radius of the entrance pupil

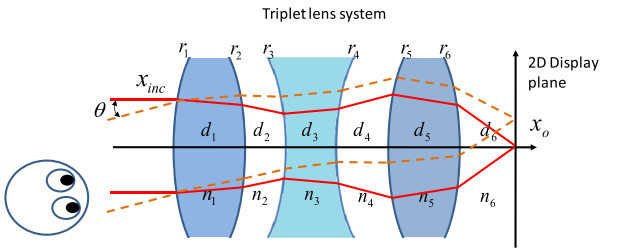

(a)

Elements of the designed merit function	
Focal spot position	$P(\theta)=\sum_i x_i I_\theta(x_i)/\sum_i I_\theta(x_i)$
Viewing angle	$Nd = 2f_{eff}\sin\theta_{\max}$
Tightness of focal spot	$V(\theta)$
Weighting factor for GA	α β

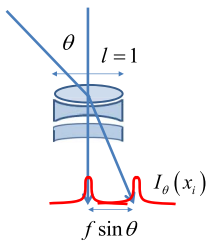

(b)

Fig. 2. (Color online) (a) Schematic of the triplet lenticular lens and (b) elements of the designed merit function of the genetic algorithm.

of the triplet lens [5]. However, practical lenses have a spread distribution of the output ray position, $x_o(x_{\text{inc}})$ as a function of x_{inc}.

The genetic algorithm [12] is employed to design the triplet lenses with a specific viewing angle and low cross talk. More precisely, it can be said that the main task is designing a short-focal-length wide-bandwidth Fourier transform lens taking the form of a triplet. The Fourier transform lens transforms the collimated ray bundle to a point source at the focal plane, while the ray bundle radiated from a point source at the focal plane is transformed to the collimated beam directed to a specific direction controlled by the lateral position of the point source [13]. Thus the point on the 2D display is observable by the someone standing at a specific direction.

In the optimization, the design of a proper merit function to be minimized is critically important. Figure 2(b) illustrates the elements of the devised merit function appropriate for the genetic algorithm and their physical concepts. In the genetic algorithm, the ray-tracing module using finite number of rays to characterize the triplet lenses is embedded. The important measures of the triplet lens as transmission efficiency, T_e, standard deviation of output ray positions, $V(\theta)$, and effective focal length f_{eff} are taken into account in the design of the merit function. The transmission efficiency T_e equals the number of output rays divided by the number of input rays. Some rays among the input rays can be rejected during the ray-tracing process by various physical blocking mechanisms, such as the vignetting effect and total internal reflection, so the transmission efficiency is less than 1. The focal spot profile for the incidence angle of θ can be characterized by the variation of the light intensity distribution defined by

$$V(\theta) = \sqrt{\frac{1}{M}\sum_{i=1}^{M} I_\theta^2(x_i) - \left(\frac{1}{M}\sum_{i=1}^{M} I_\theta(x_i)\right)^2}, \qquad (1)$$

where $I_\theta(x_i)$ is the light intensity at point x_i of the focal plane, which is equivalently measured by the number of rays accumulated at the point x_i after the ray-tracing procedure. M is the total number of uniform spatial sampled points x_i at the focal plane. As the focal spot gets tighter, the value of $V(\theta)$ becomes bigger, and reversely as the focal spot spreads, the value $V(\theta)$ becomes smaller. Thus it is desirable that the values of $V(\theta)$ are uniformly distributed or ideally constant for an arbitrary incidence angle of θ. In practical optimization, the value of $V(\theta)$ cannot be greater than an upper limit value, because the number of rays used in the ray-tracing simulation is finite. In this paper, the relevant value of $V(\theta)$ indicating the acceptable quality of the focal spot is tuned to 600. The function $P(\theta)$ of the center of the focal spot is defined by

$$P(\theta) = \sum_i x_i I_\theta(x_i) / \sum_i I_\theta(x_i). \qquad (2)$$

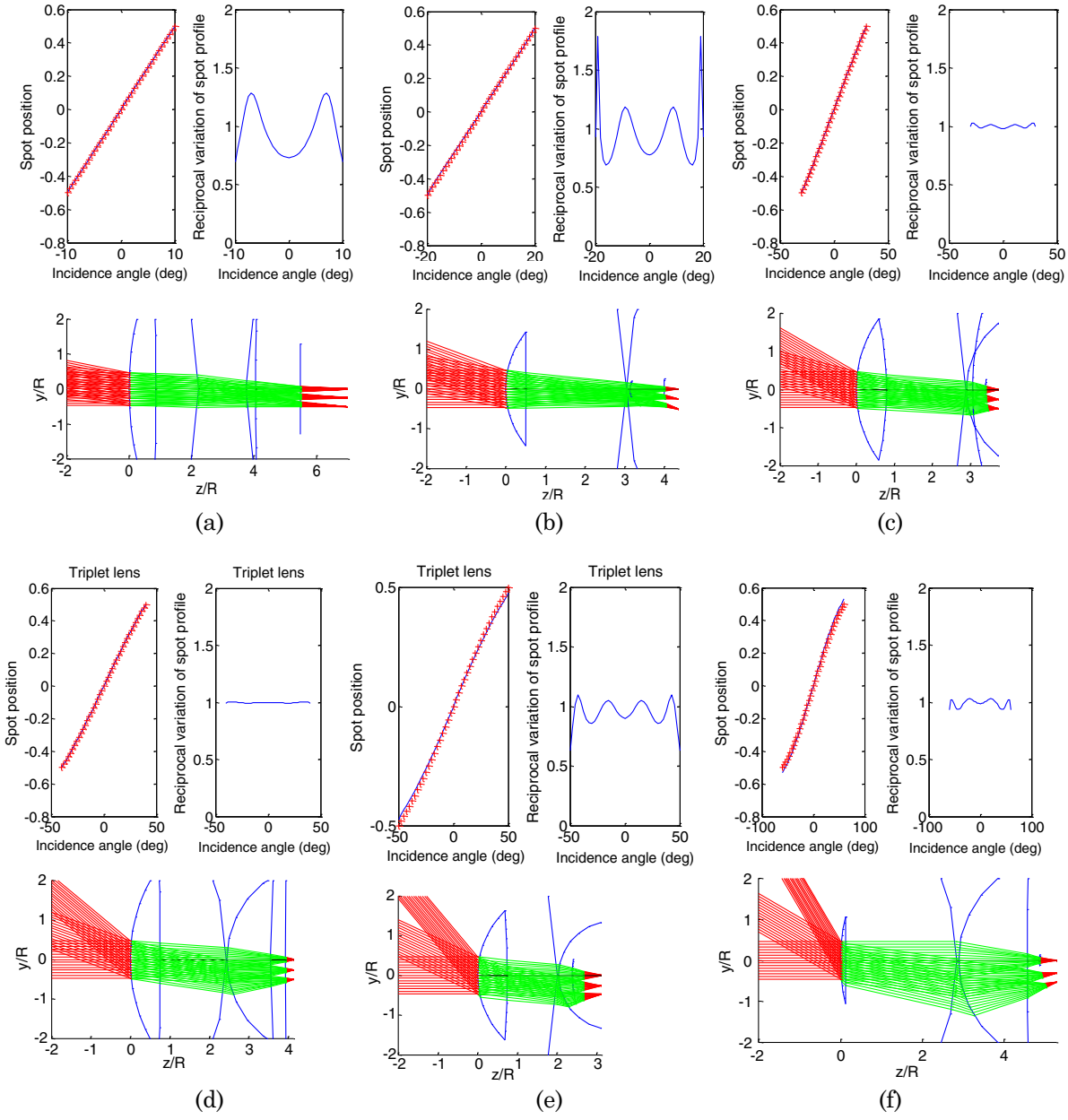

Fig. 3. (Color online) Designed triplet lenses for viewing angles of (a) 20°, (b) 40°, (c) 60°, (d) 80°, (e) 100°, and (f) 120°.

The root mean square of the difference of $P(\theta)$ and $f_{\text{eff}} \sin\theta$ is used as the measure of the accuracy of the effective focal length of the triplet lens. The merit function devised with these terms takes the form of

$$E = \begin{cases} 1,000,000 & \text{for } T_e < T_{\min} \\ \alpha\sqrt{\int_0^{\theta_{\max}(^\circ)} |1 - \frac{600}{V(\theta)}|^2 \mathrm{d}\theta} & \\ +\beta\sqrt{\int_0^{\theta_{\max}(^\circ)} |P(\theta) - f_{\text{eff}} \sin\theta|^2 \mathrm{d}\theta} & \text{for } T_e \geq T_{\min} \end{cases}. \tag{3}$$

The first term of Eq. (3) is related to the quality of the focal spot, the concept of which is illustrated by the solid red line in Fig. 2(a). The second term restricts the effective focal length of the triplet to a target value of f_{eff}. The relative weighting factors of the two terms are denoted by α and β. The final optimization result is sensitive to the choice of α and β. The values of α and β should be properly determined by repeated trial and error in practice. In addition, the transmission efficiency T_e has to be greater than a threshold value $T_e \geq T_{\min}$. This condition is necessary to exclude a meaningless solution of low transmission less than $T_{\min}$. $T_{\min}$ is set to 30% in this paper.

4. Observation Simulation of 3D Unit Pixels with Designed 3D Unit Pixel Triplet Lenses

Six triplet lenses with viewing angles of 20°, 40°, 60°, 80°, 100°, and 120° are designed by the genetic algorithm with the proposed merit function. In the

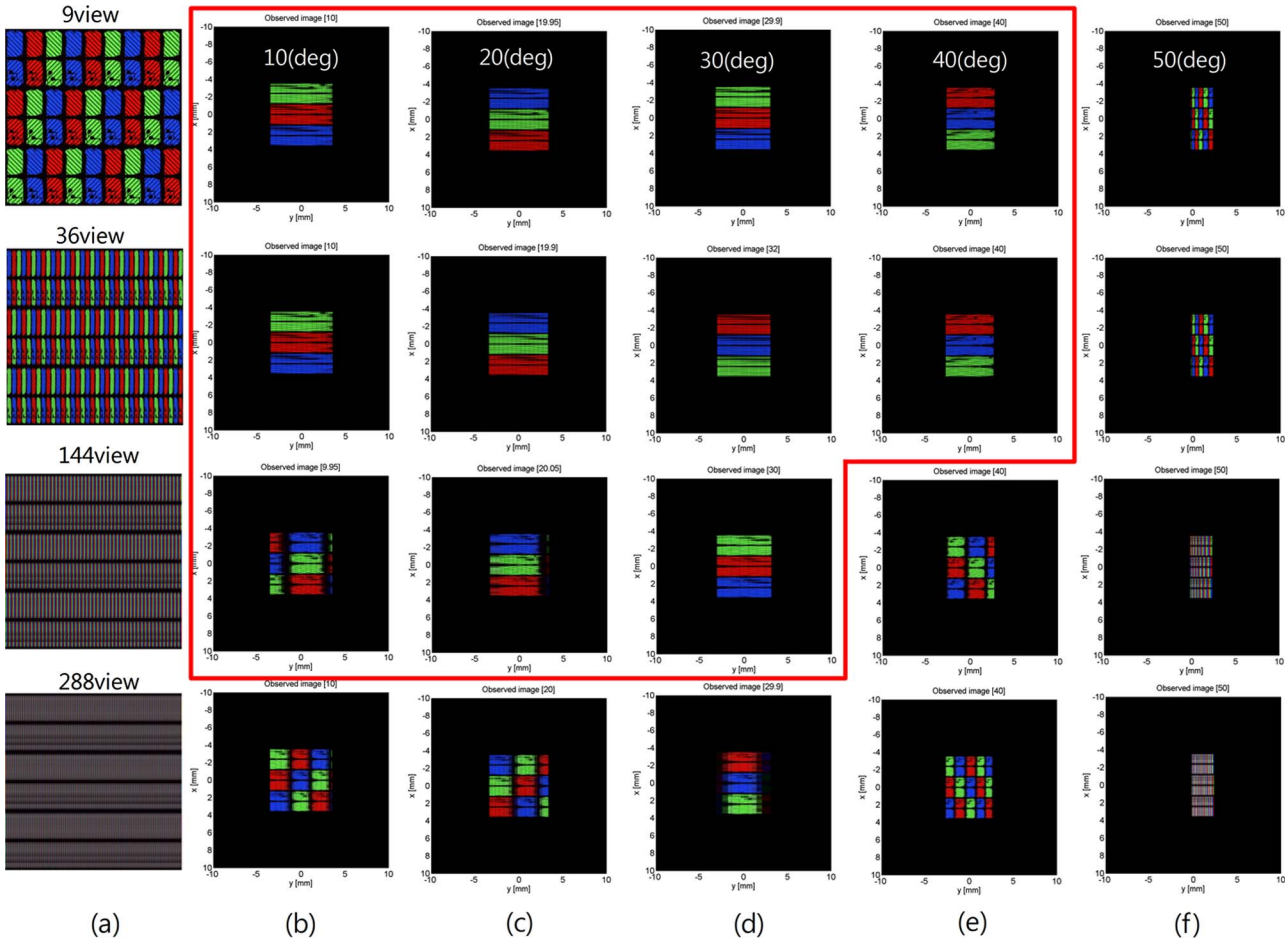

Fig. 4. (Color online) 3D pixel simulation of the designed triplet with viewing angle of 60°: (a) pixel patterns of 9-, 36-, 144-, and 288-view and simulation images of 3D unit pixels at observation angles of (b) 10°, (c) 20°, (d) 30°, (e) 40°, and (f) 50°.

optimization, the refractive index of the material is taken as freely variable in the range of from 0 to 4. In this paper, the manifestation of the theoretical limit of the potential performance of triplet lenses is mainly considered, and thus an arbitrary value of the material refractive index is allowed. Figures 3(a)–3(f) present the focusing properties and ray-tracing simulations of six designed triplet lenses, respectively. As seen in the ray-tracing simulations, the spot position (on the vertical axis) is restrictively varied within the normalized lens pitch of 1 for various incidence angles. The respective ray-tracing simulations show the superposition of ray traces for three incidence angles of 0°, $0.5\theta_{\max}(°)$, and $\theta_{\max}(°)$. The spot position versus incidence angle and the reciprocal variation of the spot profile given by $600/V(\theta)$ are plotted in Fig. 3. The inclination factor of the plot of the spot position is the effective focal length of the designed triplet lens. The flatness of the reciprocal variation reflects the cross talk level of the triplet lens. In Figs. 3(c) and 3(d), an almost perfect uniformity of the focal spot variation is obtained for a wide range of incidence angles, which means that these triplet lenses can produce wide-viewing-angle 3D images with negligible cross talk.

The performance of the 3D unit pixels equipped with the designed triplet lenses with respect to the viewing angle and cross talk is analyzed through the ray-tracing observation simulation. The simulation results of the triplet lens with viewing angles of 60° and 80° [Figs. 3(c) and 3(d)] selected among six designed triplets are presented in Figs. 4 and 5, respectively. The leftmost columns in Figs. 4 and 5 contain the 9-, 36-, 144-, and 288-view 2D pixel patterns allocated to a single 3D unit pixel. The second column in Fig. 4 presents the 3D unit pixel images observed at the observation angle of 10° for each of the pixel patterns. Whether the observation image of the 3D unit pixel is cross-talk-free or not is judged by identifying whether the observed image shows more than double the pixels of the 2D pixel pattern or not. As seen in the second column, the designed triplet lens produces significant cross talk for the 288-view pixel pattern, even at the small observation angle of 10°. However, as indicated by the red-outlined section seen in Fig. 4, except for the 288-view, to the observation angle of 30°, the 3D unit pixel with the triplet lens can display a cross-talk-free 3D pixel image successfully, which is clearly in contrast to the exemplary image of the singlet simulation shown in Fig. 1(b). For observation angles greater than

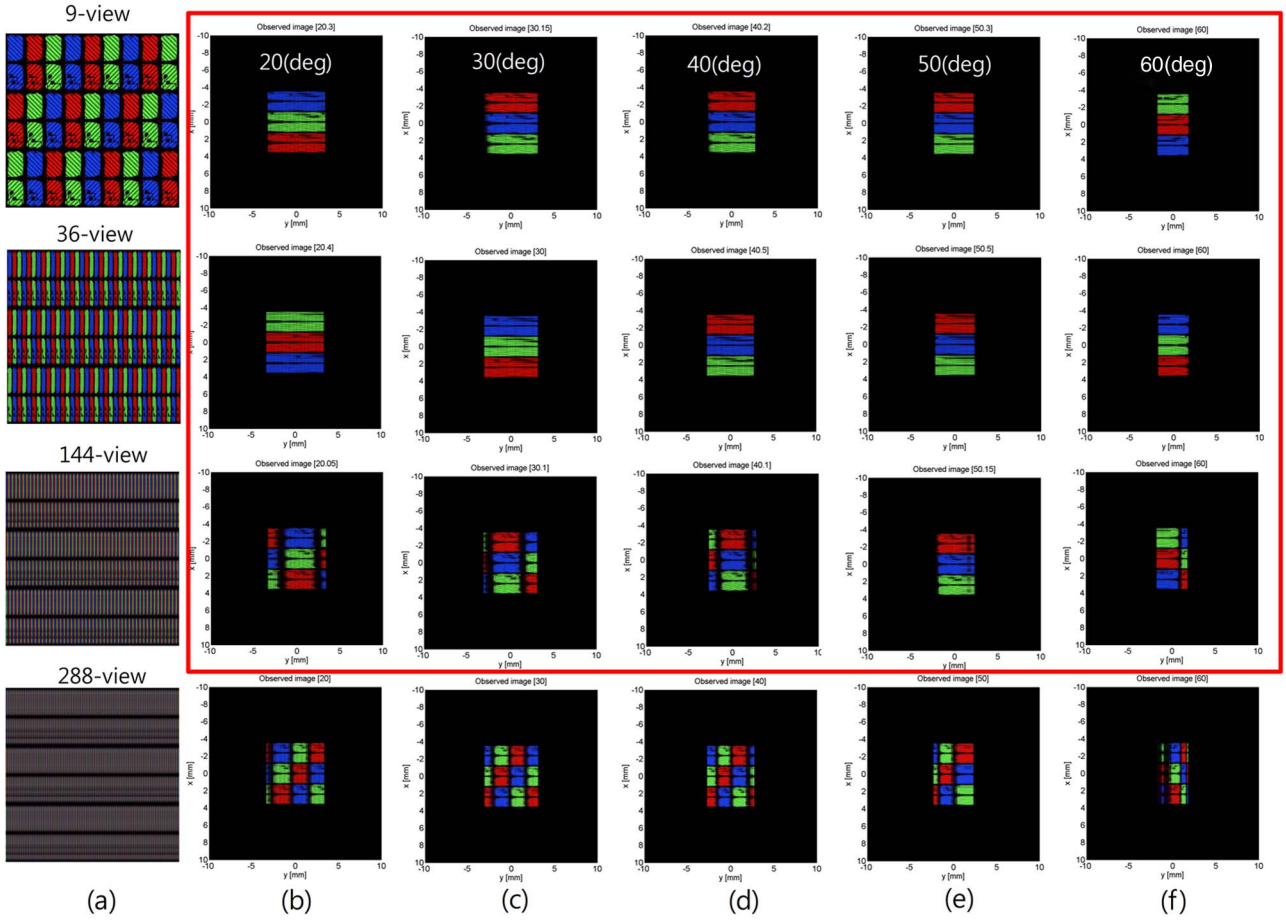

Fig. 5. (Color online) 3D pixel simulation of the designed triplet with viewing angle of 80°: (a) pixel patterns of 9-, 36-, 144-, and 288-view and simulation images of 3D unit pixels at observation angles of (b) 20°, (c) 30°, (d) 40°, (e) 50°, and (f) 60°.

30°, the observation images of the 3D unit pixels of the 144- and 288-view are contaminated by cross talk, but those of the 9- and 36-view show a cross-talk-free observation image.

Comparing the outlined areas in Figs. 4 and 5, we can see that the triplet lens with target viewing angle of 80° in Fig. 5 produces more improved results over the triplet lens with the target viewing angle of 60°. Interestingly, the target viewing angle of the triplet lens was set to 80° in the genetic algorithm, but the obtained triplet lens shows the best performance even for the observation angle of 60°, as manifested in Fig. 5. Thus the viewing angle of the obtained triplet lens can be said to have a viewing angle of 120° without cross talk. However, this triplet lens does not also provide satisfactory resolution for the 288-view pattern, as seen in Fig. 5. Further research on the special lens design is required for the 288-view lenticular 3D display.

The observation simulation of the 3D unit pixel is performed for a total of 36 cases, indicated in Fig. 6.

Viewing angle (deg)	20	40	60	80	100	120
9 views				No 3D effect		
18 views						
36 views		Binocular parallax with motion parallax				
72 views						
144 views						
288 views	supermultiview					

Fig. 6. (Color online) Classification of 3D modes with respect to the viewing angle and the number of views: pupil diameter, 5 mm; maximum acceptance angle of eye, 0.5°; observation distance, 50 cm; interpupilary distance, 65 mm; and convergence angle, 7.5°.

Viewing angle (deg)	20	40	60	80	100	120
9 views	O	O	O	O	O	O
18 views	O	O	O	O	O	O
36 views	O	O	O	O	O	O
72 views	O	O	O	O	O	O
144 views	O	O	O	O	O	O
288 views	X	X	X	X	X	X

No 3D effect

Binocular parallax with motion parallax

supermultiview

Fig. 7. (Color online) Results of design and evaluation of 3D unit pixel with triplet lens.

The overall analysis results of the six triplet lenses for the six pixel patterns are illustrated in Fig. 7, which is the filled-in version of Fig. 6. As seen in Fig. 7, it is noticeable that the supermultiview condition is obtainable with the use of the optimally designed triplet lens array. In Fig. 7, we show that the lenticular 3D display with viewing angle of 120° and 144 views without interview cross talk can be realized with the use of an optimally designed triplet lens array.

5. Concluding Remarks

We devised the optimal design method of the triplet lens for lenticular 3D displays with a wide viewing angle and low cross talk. The proposed merit function of the genetic algorithm is proven to be effective to obtain the triplet lens having the properties of reserving the tightness of the focal spot for a wide range of observation angles. The triplet lens addressed in this paper can be also useful for more general lens-based 3D displays, such as integral imaging and projection-type multiview 3D displays. Meanwhile, it would be interesting to compare the optical characteristics and functional limitations of a triplet lens array and a nonspherical singlet lens array. We will report the design of the nonspherical singlet array for achieving the same objective in a future paper, which is more relevant with respect to the feasibility of fabrication than the triplet lens array.

This work was supported by a Korea University grant.

References

1. A. Jones, I. McDowall, H. Yamada, M. Bolas, and P. Debevec, "An interactive 360° light field display," in *Proceedings of ACM SIGGRAPH 2007 Emerging Technologies* (ACM, 2007), p. 13.
2. R. Lopez-Gulliver, S. Yoshida, S. Yano, and N. Inoue, "gCubik: a cubic autostereoscopic display for multiuser interaction: grasp and group-share virtual images," in *Proceedings of ACM SIGGRAPH 2008 Posters* (ACM, 2008), p. 133.
3. Y. Kim, J.-H. Park, H. Choi, S. Jung, S.-W. Min, and B. Lee, "Viewing-angle-enhanced integral imaging system using a curved lens array," Opt. Express **12**, 421–429 (2004).
4. J. Hahn, H. Kim, Y. Lim, G. Park, and B. Lee, "Wide viewing angle dynamic holographic stereogram with a curved array of spatial light modulators," Opt. Express **16**, 12372–12386 (2008).
5. H. Kim, J. Hahn, and B. Lee, "The use of a negative index planoconcave lens array for wide-viewing angle integral imaging," Opt. Express **16**, 21865–21880 (2008).
6. H. Kim, J. Hahn, and B. Lee, "Image volume analysis of omnidirectional parallax regular-polyhedron three-dimensional displays," Opt. Express **17**, 6389–6396 (2009).
7. Y. Takaki and N. Nago, "Multi-projection of lenticular displays to construct a 256-view super multi-view display," Opt. Express **18**, 8824–8835 (2010).
8. T. Balogh, T. Forgács, T. Agocs, O. Balet, E. Bouvier, F. Bettio, E. Gobbetti, and G. Zanetti, "A scalable hardware and software system for the holographic display of interactive graphics applications," in *EUROGRAPHICS 2005 Short Papers Proceedings* (ACM, 2005), pp. 109–112.
9. C. Van Berkel and J. A. Clarke, "Characterisation and optimisation of 3D-LCD module design," Proc. SPIE **3012**, 179–187 (1997).
10. H.-J. Im, B.-J. Lee, H.-K. Hong, and H.-H. Shin, "Autostereoscopic 60 view 3D using slanted lenticular lens arrays," J. Inf. Disp. **8**, 23–26 (2007).
11. Y.-G. Lee and J. B. Ra, "Image distortion correction for lenticular misalignment in three-dimensional lenticular displays," Opt. Eng. **45**, 017007 (2006).
12. Z. Michalewicz, *Genetic Algorithms + Data structures = Evolution Programs* (Springer, 1999).
13. J. Zeng, G. Jin, M. Wang, Q. He, and Y. Yan, "Design of a short-focal-length double-Fourier-transform-lens system for holographic storage," Opt. Eng. **46**, 033002 (2007).